The Astrophysical Journal, 881:52 (10pp), 2019 August 10 https://doi.org/10.3847/1538-4357/ab2b99

Dynamic Evolution of Current Sheets, Ideal Tearing, Plasmoid Formation and Generalized Fractal Reconnection Scaling Relations

K. A. P. Singh[1,2], Fulvia Pucci[3,4], Anna Tenerani[5], Kazunari Shibata[2], Andrew Hillier[6], and Marco Velli[7]

[1] Department of Physics, Institute of Science, BHU, Varanasi 221005, India; alkendra.solarastrophysics@gmail.com, singh@kwasan.kyoto-u.ac.jp

[2] Astronomical Observatory, Graduate School of Science, Kyoto University, Yamashina, Kyoto 607-8471, Japan

[3] NINS, National Institutes of Natural Sciences, 105-0001, Minato City, Tokyo, Japan

[4] Princeton Plasma Physics Laboratory, Princeton University, Princeton, NJ 08543-0451, USA

[5] Department of Physics, University of Texas, Austin, TX 78712, USA

[6] Department of Mathematics, CEMPS, University of Exeter, Exeter EX4 4QF, UK

[7] Department of Earth, Planetary, and Space Sciences, UCLA, Los Angeles, CA 90095, USA

Received 2019 February 5; revised 2019 June 1; accepted 2019 June 19; published 2019 August 12

Abstract

Magnetic reconnection may be the fundamental process allowing energy stored in magnetic fields to be released abruptly, with solar flares and coronal mass ejection being archetypal natural plasma examples. Magnetic reconnection is much too slow of a process to be efficient on the large scales, but accelerates once small enough scales are formed in the system. For this reason, the fractal reconnection scenario was introduced to explain explosive events in the solar atmosphere; it was based on the recursive triggering and collapse via tearing instability of a current sheet originally thinned during the rise of a filament in the solar corona. Here we compare the different fractal reconnection scenarios that have been proposed, and derive generalized scaling relations for the recursive triggering of fast, "ideal" —i.e., Lundquist number independent—tearing in collapsing current sheet configurations with arbitrary current profile shapes. An important result is that the Sweet–Parker scaling with Lundquist number, if interpreted as the aspect ratio of the singular layer in an ideally unstable sheet, is universal and does not depend on the details of the current profile in the sheet. Such a scaling, however, must not be interpreted in terms of stationary reconnection, rather it defines a step in the accelerating sequence of events of the ideal tearing mediated fractal cascade. We calculate scalings for the expected number of plasmoids for such generic profiles and realistic Lundquist numbers, showing that in ideal tearing scenarios a smaller number of plasmoids, by orders of magnitude, is generated compared to the original fractal model.

Key words: magnetic reconnection – magnetohydrodynamics (MHD) – plasmas

1. Introduction

Magnetic reconnection is a dynamical mechanism pervasive in the high-temperature, low-resistivity plasmas common in astrophysical settings as well as in the laboratory in fusion research. It is considered to be one of the most fundamental processes permitting mass, momentum, and energy transfer (Zweibel & Yamada 2009; Yamada et al. 2010; Pontin 2011; Shibata & Magara 2011; Daughton & Roytershteyn 2012). If energy is to be released through the process of magnetic reconnection, then it has to be stored in the magnetic field in the initial stage, so reconnection must be an off/on process, and cannot be occurring on any kind of fast timescale all of the time. If this were not the case, stars and accretion disks would not have coronae, the magnetic dynamo would not work, and there would be no supersonic solar wind (see, e.g., Zweibel & Yamada 2009; Yamada et al. 2010). A complete understanding of magnetic reconnection therefore requires explaining how energy accumulates in the magnetic field, how current carrying fields becomes unstable, and how magnetic energy release occurs on short timescales once the reconnection process has been triggered.

A major difficulty in the understanding of the magnetic reconnection stems from the fact that classical models of reconnection starting from the steady state Sweet–Parker (SP) mechanism (Parker 1957; Sweet 1958), or the non-steady, resistive instabilities (Furth et al. 1963) appeared to be inadequate to explain the observed, transient, and explosive release of the magnetic energy in various plasma environments. The fast steady state mechanism proposed by Petscheck (Petschek 1964), with a short diffusive region emanating slow mode shocks was shown in numerical simulations to depend intrinsically on non-uniform or anomalous local resistivities and impossible to achieve with quasi-uniform plasma parameters. Because reconnection is a locally small-scale phenomenon strongly influenced by global conditions, it remains a difficult topic to fully understand. The extremely large values of the magnetic Reynolds and Lundquist numbers of high-temperature plasmas mean that the scales where reconnection occur may become so small that the mechanism allowing magnetic field topology change may not be tied to resistivity at all but to kinetic effects (see, e.g., Drake & Kleva 1991; Ottaviani & Porcelli 1993; Hesse et al. 2001; Singh et al. 2015; Del Sarto et al. 2016; Pucci et al. 2017).

As had been pointed out already by Biskamp (1986), the SP current sheet becomes unstable in numerical simulations with sufficiently high resolution, to a very fast reconnecting mode. Here higher resolution corresponds to higher Lundquist numbers and when these Lundquist numbers became sufficiently high, the effect of inflow/outflow on the current sheet becomes negligible compared to the effect of the tearing mode (Shi et al. 2018). This instability of the SP sheet (Tajima & Shibata 2002; Loureiro et al. 2007) was called the super-tearing mode and then the plasmoid instability, as it leads both to a growth rate that increases with the Lundquist number, and to a large number of magnetic islands, or plasmoids, being formed. Many further works were devoted to studying the SP plasmoid

instability (e.g., Huang & Bhattacharjee 2010, 2013; Huang et al. 2011; Loureiro et al. 2013), investigating its formation and the scaling of the number of islands formed with Lundquist number.

Pucci & Velli (2014), hereafter PV14, noted that the main result for tearing on SP sheets, namely that the growth rate increased with increasing Lundquist number, would lead to a catastrophe in the ideal limit. PV14 therefore conjectured that in the "ideal" limit of high Lundquist numbers, as a current sheet thinned, magnetic reconnection would survive, but the tearing mode growth rate would become at most independent of Lundquist number. In other words, current sheets as thin as SP would never form, but reconnection would occur at thicker aspect ratios. PV14 also discussed their neglect of flow structure in the stability analysis: in their reasoning, only current sheets with SP aspect ratios require consideration of flows, as they are required to sustain the sheets that would otherwise diffuse away on an ideal timescale.

Defining the Lundquist number $S = LV_a/\eta$, with L being the sheet half-length, V_a the Alfvén speed, and η the magnetic diffusivity, an SP sheet has an inverse aspect ratio $a/L \sim S^{-1/2}$, while PV14 found that tearing becomes "ideal" at $a/L \sim S^{-1/3}$. In addition, they pointed out that the nonlinear dependence of the growth rate on the current sheet aspect ratio could explain several phenomena in which magnetic reconnection exhibits an explosive character, in the sense that magnetic energy can be stored over a long period of time and then suddenly released on a timescale comparable with the macroscopic ideal Alfvén time. The first simulations of the instability of a sheet of this aspect ratio were carried out by Landi et al. (2015), while Tenerani et al. (2015a) extended the analysis of PV14 and studied the role of viscosity on the tearing mode instability of thin current sheets. The scalings found by PV14 are modified in the presence of viscosity, which allows thinner sheets to remain stable.

Shibata & Tanuma (2001) developed the plasmoid-induced reconnection model, considered fractal tearing, and found a similar criterion $a/L \leqslant S^{-1/3}$ for the fast tearing instability following a different line of thought. Inspired by the fact that the stationary SP current sheet is stable at small Lundquist number precisely due to the outflow of material accelerated to the Alfvén speed along the sheet (Shi et al. 2018), the question that Shibata & Tanuma (2001) asked is for what aspect ratio the growth time of the instability timescale τ_g becomes shorter than the evacuation time along the sheet $\tau_g \leqslant L/V_a$. Because the evacuation time does not depend on the Lundquist number, equality is obtained when the growth rate (or time) also becomes independent of the Lundquist number, and therefore the limiting criterion yields the same aspect ratio scaling as PV14.

Shibata & Tanuma (2001) and Singh et al. (2015) pointed out that the magnetic reconnection is strongly time dependent and bursty, and the role of fractal-like tearing is to produce a very thin current sheet with a microscopic scale of the order of the ion-Larmor radius or the ion-inertial length. The main energy release, however, is explained by a recursive fast reconnection process which occurs after the ejection of the large-scale plasmoid: this fractal magnetic reconnection model of Shibata & Tanuma (2001) suggests that the impulsive bursty regime of reconnection is associated with a series of plasmoids formation and subsequent ejections on various scales; in fact, Nishizuka et al. (2010) report seven plasmoid ejections associated with an impulsive burst of hard X-ray emission. The time-dependent nature of magnetic reconnection was noticed in three-dimensional magnetohydrodynamics (MHD) simulations by Nishida et al. (2013); it was found that an SP type steady current sheet (at low Lundquist number) is formed below a rising flux rope. The thinning of the current sheet continues due to the rising of the flux rope until the current sheet becomes sufficiently thin so that it becomes either unstable for the tearing instability or the anomalous resistivity sets in. During this time, the current sheet is fragmented into several small-scale current sheets, with multiple x-lines and o-lines, where current density is present as well as locally enhanced.

Tenerani et al. (2015b), in simulations of a collapsing sheet aimed at testing the PV14 critical aspect ratio, also observed nonlinear recursive evolution of collapsing x-points and, inspired by the Shibata & Tanuma (2001) model, developed a similar but different analytical description of the recursive collapse. A recent review on the instability of current sheets and triggering of fast magnetic reconnection can be found in Tenerani et al. (2016).

More recently, it has been shown how the critical aspect ratio scalings of PV14 change when equilibrium configurations different from the Harris current sheet profiles are considered. In particular, Del Sarto et al. (2016) discussed this issue while examining kinetic extensions of the ideal tearing (IT) concept, and included the theoretical prediction of the resistive maximum growth rate scaling, while Pucci et al. (2018) investigated the resistive IT in the case of a boundary field and double current sheet configurations, confirming numerically the scaling of the maximum growth rate. In the present work, we first briefly summarize the properties of the tearing instability of thin current sheets for arbitrary aspect ratios in Section 2. In Section 3, we compare the fractal reconnection scenarios developed by Shibata & Tanuma (2001) and Tenerani et al. (2015b), which are then generalized by incorporating arbitrary current sheet profiles in the stability calculations and recursive relations. Finally, the conclusions discuss the possible implications for models of turbulent reconnection as well as three-dimensional effects.

2. A Summary of the Tearing Mode for Current Sheets with General Gradients

The dispersion relation for the reconnecting instability of a one-dimensional current sheet structure in which the magnetic field reverses sign, i.e., it is odd across the sheet, while the current is even, depends, in resistive MHD, on the magnetic diffusivity η, the shear-scale a defining the current sheet thickness, the wavenumber ka, and the equilibrium structure, aligned here with the x-direction, i.e., the $\hat{i}$-direction, and dependent only on the y-coordinate, i.e., the $\hat{j}$- direction, defined through the relation

$$\vec{B}(y) = B(y)\hat{i} = B_0 F\left(\frac{y}{a}\right)\hat{i}, \tag{1}$$

where F is an arbitrary odd nondimensional function whose first derivative provides the current profile. B_0 is an estimate of the maximum field strength (for the Harris current sheet $F = \tanh(y/a)$, B_0 is also the value of the field far from the sheet). The linear stability (for incompressible fluctuations) does not depend on the presence or absence of a magnetic field

in the third orthogonal direction (z or $\hat{k}$) and whether the equilibrium is force-free or pressure balanced. The detailed profile of F enters the dispersion relation by determining the famed Δ' parameter, which is the jump in the gradient of the reconnecting perturbed magnetic field component $\tilde{b}_y$ across the current sheet, as obtained by solving the corresponding component of the perturbed momentum equation assuming ideal MHD and a vanishing growth rate. At large Lundquist number ($\eta \to 0$), analysis of the solutions to the linearized equations, subject to the boundary conditions that the velocity and magnetic field perturbations vanish far from the sheet, show that two regions define the solution structure: a boundary layer of thickness 2δ around the center ($y = 0$) of the current sheet, and outer regions where diffusivity and growth rate may be neglected—as stated for the Δ' calculation. For the Harris sheet case, Δ' is given by the expression

$$\Delta' = a\frac{b'_y(0^+) - b'_y(0^-)}{b_y(0)} = 2\left(\frac{1}{ka} - ka\right). \tag{2}$$

In order to have instability, Δ' must be greater than 0. Two asymptotic expressions summarize the dispersion relation, depending on whether $\Delta'\delta/a \ll 1$ (small Delta prime or Δ', subscript SD)

$$\begin{aligned}\gamma_{\rm SD}\bar{\tau}_A &\simeq A^{\frac{4}{5}}\bar{k}^{\frac{2}{5}}(\Delta')^{\frac{4}{5}}\bar{S}^{-\frac{3}{5}}\\ \delta_{\rm SD}/a &\sim (\bar{S}\bar{k})^{-\frac{2}{5}}(\Delta')^{\frac{1}{5}},\end{aligned} \tag{3}$$

where A is a nondimensional constant, or $\Delta'\delta/a \gg 1$ (large Delta prime or Δ', subscript LD)

$$\gamma_{LD}\bar{\tau}_A \simeq \bar{k}^{\frac{2}{3}}\bar{S}^{-\frac{1}{3}}\ \delta_{LD}/a \sim (\bar{S}\bar{k})^{-\frac{1}{3}}, \tag{4}$$

in which case the growth rate no longer depends explicitly on Δ' (Del Sarto et al. 2016; Pucci et al. 2018). Here, barred quantities are normalized to the current sheet thickness ($\bar{\tau}_A = a/V_{\rm a}$, $\bar{k} = ka$, $\bar{S} = aV_{\rm a}/\eta$). The expressions above may be used to find the scaling of the fastest growing mode by assuming that both relations remain valid at the wavenumber of maximum growth $k_m(\bar{S})$ for sufficiently large $\bar{S}$. As the Lundquist number grows, the wavenumber of maximum growth continues to decrease, and in the expression for Δ' the only part of interest is the dependence on wavenumber as $ka \to 0$. For the Harris current sheet this implies $\Delta' \sim 2/ka$, leading to

$$\gamma\bar{\tau}_{\rm A} \sim \bar{S}^{-\frac{1}{2}},\ \frac{\delta}{a} \sim \bar{S}^{-\frac{1}{4}},\ k_m a \sim \bar{S}^{-\frac{1}{4}}. \tag{5}$$

PV14 rescaled the dispersion relation to current sheet half-length rather than half-thickness and times normalized to the Alfvén time along the sheet (i.e., unbarring the Lundquist number and Alfvén time):

$$\begin{aligned}\gamma\tau_{\rm A} &\sim S^{-\frac{1}{2}}\left(\frac{a}{L}\right)^{-\frac{3}{2}},\ \frac{\delta}{L} \sim S^{-\frac{1}{4}}\left(\frac{a}{L}\right)^{\frac{3}{4}},\\ k_m L &\sim S^{-\frac{1}{4}}\left(\frac{a}{L}\right)^{-\frac{5}{4}}.\end{aligned} \tag{6}$$

PV14 then argued, assuming an inverse aspect ratio of the form $a/L \sim S^{-\alpha}$, that any value of $\alpha < 1/3$ would lead to a divergence of growth rates in the ideal limit, while any value of $\alpha > 1/3$ would lead to growth rates that tend to zero as the Lundquist number grows without bounds. In order to preserve a physically consistent ideal MHD limit, PV14 therefore argued that $\alpha = 1/3$ was a critical exponent at which inverse aspect ratio current sheets would continue to tear, at the ideal rate, when $S \to \infty$. They also pointed out how the nonlinear dependence of the growth rate on the aspect ratio could allow the tearing mode to provide a trigger for non-ideal explosive events.

The expressions in Equations (5), (6) may be generalized to other equilibria by allowing for a different function Δ', and more specifically with its functional dependence on ka, in the limit of small ka (the small Δ' regime). For small values of ka, what is important is that we may assume $\Delta' \sim (ka)^{-p}$ with $p > 0$ (see Pucci et al. (2018) for an example of a current sheet with vanishing far field that leads to $p = 2$, as well as a more general discussion including, for example, a double current sheet and different boundary conditions). This leads to the generalized fastest growing mode dependencies

$$\gamma\bar{\tau}_{\rm A} \sim \bar{S}^{-\frac{1+p}{1+3p}},\ \frac{\delta}{a} \sim \bar{S}^{-\frac{p}{1+3p}},\ k_m a \sim \bar{S}^{-\frac{1}{1+3p}}. \tag{7}$$

Notice that such scalings imply that the exponents of power-law dependencies on growth rate etc. do not have a large domain of variation. The maximum growth rate scales with Lundquist number with an exponent between $-1/2$ (i.e., for $p = 1$) and $-1/3$ (i.e., for $p \to \infty$), and the singular layer thickness scaling exponent varies between $-1/4$ (i.e., for $p = 1$) and $-1/3$ (i.e., for $p \to \infty$).

Again, rescaling the dispersion relation to current sheet half-length rather than thickness, and normalized to the Alfvén time along the sheet (i.e., unbarring the Lundquist number and Alfvén time):

$$\begin{aligned}\gamma\tau_{\rm A} &\sim S^{-\frac{1+p}{1+3p}}\left(\frac{a}{L}\right)^{-2\frac{1+2p}{1+3p}},\ \frac{\delta}{L} \sim S^{-\frac{p}{1+3p}}\left(\frac{a}{L}\right)^{\frac{1+2p}{1+3p}},\\ k_m L &\sim S^{-\frac{1}{1+3p}}\left(\frac{a}{L}\right)^{-\frac{2+3p}{1+3p}}.\end{aligned} \tag{8}$$

From these relations one can then find the critical exponents for the current sheet aspect ratio at which the growth rates no longer depend on the Lundquist number, i.e., for which relationship between a/L and S the growth rate is independent of S

$$\frac{a}{L} \sim S^{-\frac{1+p}{2(1+2p)}}, \tag{9}$$

where again the exponent can only vary between $-1/3$ (i.e., for $p = 1$) and $-1/4$ (i.e., for $p \to \infty$). Similarly one finds the scalings of the maximum growth wavenumber and of the singular layer thickness with the Lundquist number S

$$k_m L \sim S^{\frac{p}{2(1+2p)}},\ \frac{\delta}{L} \sim S^{-\frac{1}{2}}. \tag{10}$$

From this we can remark that, while for the wavenumber of maximum growth the exponential dependence on S varies between $1/6$ (i.e., for $p = 1$) and $1/4$ (i.e., for $p \to \infty$), the singular layer thickness (or inverse aspect ratio) is universal and equilibrium independent, scaling precisely as the SP current sheet inverse aspect ratio. Note that, in their analysis of

the instability of secondary current sheets driven by a large-scale primary instability, Del Sarto & Ottaviani (2017) and Del Sarto et al. (2018) found a similar result when including the effects of embedded current sheets (discussed further below). The fact that the singular layer thickness is universal and equilibrium independent may seem surprising at first sight, but is actually a simple consequence of the requirement that the tearing mode instability proceeds on ideal timescales. As remarked by PV14, such an aspect ratio is the only one that allows dissipation to balance the perturbed inflowing magnetic energy, even in the presence of a growing mode. It might also be one of the reasons numerical simulations tend to identify sheets with inverse aspect ratios scaling à la SP as seen in e.g., Cassak & Drake (2009), Huang & Bhattacharjee (2010), Servidio et al. (2010), Baalrud et al. (2011), and Huang et al. (2017)—the last paper confirming the impossibility of SP sheet formation at large S—though the ratio of outflow to inflow velocities for the instability does not satisfy the proper SP scaling. Indeed it is easy to see that incompressibility implies that the ratio of outflow to inflow velocities at the x-point scales, in the presence of an ideally growing tearing mode, as

$$V_{\rm in}/V_{\rm out} \sim S^{-\frac{(1+p)}{2(1+2p)}}, \tag{11}$$

and is larger than the stationary SP inflow/outflow ratio, scaling with an exponent monotonically decreasing with p between one-third and one-fourth. In other words, for a growing tearing mode there is a larger ratio of inflow to outflow, as required by an exponentially increasing reconnection rate in the linear phase of the instability.

3. Fractal Reconnection Scenarios Compared

The scenario where a fast reconnection instability would disrupt current sheets whose inverse aspect ratio was small enough had already been observed in numerical simulations by Biskamp (1986). This process was discussed in more detail in terms of multiple plasmoid formation by Tanuma et al. (1999, 2001) and Shibata & Tanuma (2001), who used the term "secondary tearing instability". For SP current sheets, Samtaney et al. (2009) and Loureiro et al. (2013) provided studies showing their violent instability to super-Alfvénic fast formation of plasmoid chains. Indeed it was the singularity and non-causality implied by the Lundquist number scaling that led Pucci & Velli 2014 to conclude that the SP current sheet may not form in the beginning (Lapenta 2008; Shibata & Takasao 2016). The presence of many plasmoids in a long and thin current sheet makes the current sheet more unstable and the overall reconnection process evolves in a strongly time-dependent manner (Tajima & Shibata 2002). The recursive reconnection scenarios that we compare here are all based upon the realization that SP sheets are never attained, but rather a scenario we have called "ideal tearing" (IT) holds (e.g., Landi et al. 2015; Tenerani et al. 2015b, 2016).

Tanuma et al. (1999, 2001) and Tanuma & Shibata (2005) conducted several MHD based numerical experiments on reconnection in current sheets, including different models for the resistivity; the fundamental results from these simulations are summarized below:

(i) The initial current sheet considered in the beginning of the simulation (or reconnection) is macroscopic, not a stationary SP current sheet, and the current sheet evolves by thinning from the start of the simulation.

(ii) When magnetic reconnection begins, in the presence of uniform resistivity, reconnection appears to be well described by the SP scaling.

(iii) Once the thinned current sheet becomes unstable to tearing, plasmoid formation occurs and smaller scales are achieved. If anomalous resistivity is allowed to set in (i.e., local regions of lower Lundquist number), reconnection becomes Petschek like.

The numerical results of Tanuma et al. (1999, 2001) inspired the fractal reconnection model described by Shibata & Tanuma (2001). Starting from the observation that magnetic reconnection occurs in a strongly time dependent and nonlinear manner, it describes an overall process that proceeds through stages during which the current sheet aspect ratio keeps changing before successive plasmoid formation in the current sheet, at smaller and smaller scales, sets in.

3.1. The Shibata Fractal Reconnection Model

The Shibata & Tanuma (2001) model starts from Harris-type current sheet profiles ($p = 1$ in the notation of the previous section), observing that for a current sheet in which inflows and outflows are present, instability requires that the tearing mode timescale (corresponding to maximum growth rate) should be smaller than the time required for the outflow to carry the perturbation out of the current sheet. Tearing of the current sheet occurs once the instability criterion is satisfied (see Equation (12)). Using the same notation as in the previous section, barred nondimensional quantities are normalized using the current sheet half-thickness a, while nonbarred quantities are normalized to the current sheet half-length L. Consider a current sheet that breaks up, with x-points collapsing to give rise to secondary current sheets, in a step-by-step process until kinetic or dissipation scales are reached. The thicknesses, Lundquist numbers, Alfvén times, etc. at the $n^{\rm th}$ step of this cascade will be denoted with the subscript n.

In the Shibata & Tanuma (2001) scenario, the current sheet at the $n^{\rm th}$ step becomes unstable to plasmoid instability if

$$t_n \leqslant L_n/V_{\rm a}, \tag{12}$$

where $t_n = 1/\gamma_n$ is the maximum growth time of the tearing mode instability; from Equation (5)

$$\gamma_n \sim \bar{S}_n^{-1/2}\bar{\tau}_{An}, \tag{13}$$

upon renormalization, as in the previous section, the inequality Equation (12) leads to

$$\frac{a_n}{L_n} \leqslant S_n^{-1/3}, \tag{14}$$

note the similarity to PV14 and Equation (9) with $p = 1$ for the upper bound of the inverse aspect ratio: the SP current sheet satisfies the inequality but with a much smaller inverse aspect ratio. Derived by comparing the Alfvén time (i.e., $L_n/V_{\rm a}$) with tearing time (corresponding to maximum growth rate of tearing mode instability), at a particular step (see Shibata & Tanuma 2001), the upper limit corresponds to a process occurring on the ideal timescale of current sheet evacuation, on the assumption that an Alfvénic outflow is present.

At the next step, in the Shibata & Tanuma (2001) model, the length of current sheets newly born out of the x-points is fixed

by the most unstable wavelength of the tearing mode in the previous step. Consider, if Equation (14) is satisfied, the expression for the fastest growing wavenumber i.e., Equation (10) and ($p = 1$), the wavelength of the fastest growing mode is given by $\lambda = 2\pi/k_m$, leading to

$$L_{n+1} = \pi L_n S_n^{-1/6}. \tag{15}$$

The number of x-points (and o-points, each of which gives rise to a plasmoid) created in the first step in a critical current sheet of Lundquist number S is then $n_1 \leqslant L_1/L_2 = S^{1/6}/\pi$.

On the other hand, the destabilization of the new sheet occurs at a thickness such that

$$\frac{a_{n+1}}{L_{n+1}} \leqslant S_{n+1}^{-1/3} = S_n^{-1/3}\left(\frac{L_{n+1}}{L_n}\right)^{-1/3} = \pi^{-1/3} S_n^{-5/18}. \tag{16}$$

Assuming equality we then get a recursive relation for the Lundquist number and current sheet thicknesses

$$S_{n+1} = \pi S_n^{5/6} \text{ or } S_{n+1} = (\pi)^{6(1-(5/6)^n)} S_1^{(5/6)^n},$$
$$\text{and } \frac{a_n}{a_{n+1}} = \left(\frac{1}{\pi}\right)^{(2/3)} S_n^{1/9}. \tag{17}$$

For $S_n = 10^{12}$, $L_n/L_{n+1} \simeq 32$ and $S_n = 10^6$, $L_n/L_{n+1} \simeq 3.2$. The ratios of current sheet width at two consecutive levels of tearing i.e., a_n/a_{n+1} for $S_n = 10^{12}$ and $S_n = 10^6$ are 10 and 2.16, respectively. This fractal process should continue until the current sheet thickness—or rather the singular layer of a tearing mode step—either reaches the first microscopic scale, such as the ion-Larmor radius or ion-inertial length, or a value for the collisional Lundquist number is sufficiently small enough to stabilize tearing completely, i.e., a value $S_N \simeq 10^4$ or less (Shi et al. 2018). The Equation (17) shows that when starting from a Lundquist number $S_1 = 10^{12}$ it takes 13 (12 excluding the initial sheet) steps to get to $S_{13} \simeq 10^4$.

The expected total number of x-points generated after M steps then becomes

$$N_M = N_1 \cdot N_2 \cdot N_3 \ldots\ldots \cdot N_M \leqslant \frac{1}{\pi} S_1^{1/6} \frac{1}{\pi} S_2^{1/6} \ldots\ldots \frac{1}{\pi} S_M^{1/6} = \left(\frac{1}{\pi}\right)^{6(1-(5/6)^M)} S_1^{(1-(5/6)^M)}. \tag{18}$$

Calculating the total number of plasmoids requires an assumption on the relationship between x-points at each step, o-points, and the behavior of islands generated at previous steps. In principle, one should sum over N_M from $M = 1$ through a final step to obtain an upper limit on the number of plasmoids. Here we will consider N_M to be a reasonable estimate for the total number of islands formed, given that larger islands will merge during the cascade. Assuming the cascade reaches down to $M = 13$ before it stabilizes we get a total number of plasmoids $N_{13} \simeq 1.5 \times 10^8$, an enormous number. Using slightly smaller values of the initial Lundquist number led Shibata & Tanuma (2001) to conclude that the number of steps should be $M \geqslant 6$ (or 5, starting from an initial sheet with $M = 1$). The number of plasmoids as a function of the number of steps and $S_1 = 10^{11}$, is shown in Figure 2.

3.2. The Tenerani et al. Fractal Reconnection Model

Tenerani et al. (2015b, 2016) carried out a series of simulations of collapsing current sheets of the Harris type with the aim of testing the PV14 critical aspect ratio criterion. To this end, Tenerani et al. (2015b, 2016) introduced a slowly collapsing primary sheet, and indeed observed that, once the aspect ratio thinned to a scale of order $a/L \sim S^{-1/3}$, a fast (plasmoid) type instability occurred. They observed the subsequent collapse of secondary x-points into further current sheets, and, inspired by Shibata & Tanuma (2001) went on to model the recursive collapse. The main difference however was that Tenerani et al. (2015b) observed that collapsing x-points had the property of maintaining their thickness unaltered while the outflow tended to lengthen them, until their inverse aspect ratio became sufficiently small that a new tearing instability was triggered. An example from their MHD simulations is shown in Figure 1, where magnetic field lines and current density are shown at $t = 26\tau_A$, $t = 27\tau_A$, and $t = 27.37\tau_A$ in the evolution. At $t = 26\tau_A$, there are many plasmoids in a long and thin current sheet. As time goes on, the current sheet lengthening is observed at $t = 27\tau_A$, e.g., for x/L between 2.7 and 3.7. At $t = 27.37\tau_A$, the plasmoids merging takes place and it can be seen clearly, e.g., for x/L between 1.7 and 2.5. So, in proceeding from the top to bottom panels, we see x-point collapsing, current sheets lengthening, and subsequent collapse, while the plasmoids formed at previous steps grow and merge.

Each subsequent x-point collapse was identified as the next step in the IT cascade because the new aspect ratios empirically satisfied the IT criterion with Lundquist numbers calculated on the new current sheet lengths. In other words, the thickness of the current sheet developing at the $n + 1$-th stage of the instability, corresponded to the inner, singular, diffusion layer of the n-th tearing mode, i.e., δ_n to be obtained from Equation (10) with $p = 1$: as new x-points collapse, they form sheets that broaden essentially at the upstream magnetic field Alfvén speed, and the current sheet thickness at stage $n + 1$ is given by $a_{n+1} = \delta_n$. In order to become ideally unstable, the current sheets have to reach a length L_n, such that their growth rate is independent of the Lundquist number calculated on the upstream magnetic field Alfvén speed and on the new half-length L_n, so that

$$\frac{a_n}{L_n} \sim S_n^{-1/3}, \tag{19}$$

and recalling the definition of a_n, one finds $a_{n+1}/L_{n+1} = \delta_n/L_{n+1} = (L_n/L_{n+1}) \cdot (S_n^{-1/2}) = S_{n+1}^{-1/3}$. Note that because the IT tearing is a scaling relation, equality is up to a constant c of $O(1)$ appearing in front of the expressions (i.e., we should write $a_n/L_n = c_n S_n^{-1/3}$ with $c_n \sim O(1)$). We omit such constants here in favor of a less cumbersome notation.

From the definition of S_n and assuming the diffusivity and the upstream magnetic field to remain the same at each level (as we have done implicitly in the previous section as well), we have (our initial sheet is labeled by $n = 1$) $S_{n+1} = (L_{n+1}/L_n) \cdot S_n$, so that

$$(L_n/L_{n+1}) \sim S_{n+1}^{1/3} \rightarrow S_n = S_1^{(3/4)^{n-1}}, \; n \geqslant 1. \tag{20}$$

The present model, inspired by the observed behavior of collapsing x-points in numerical simulations, leads to

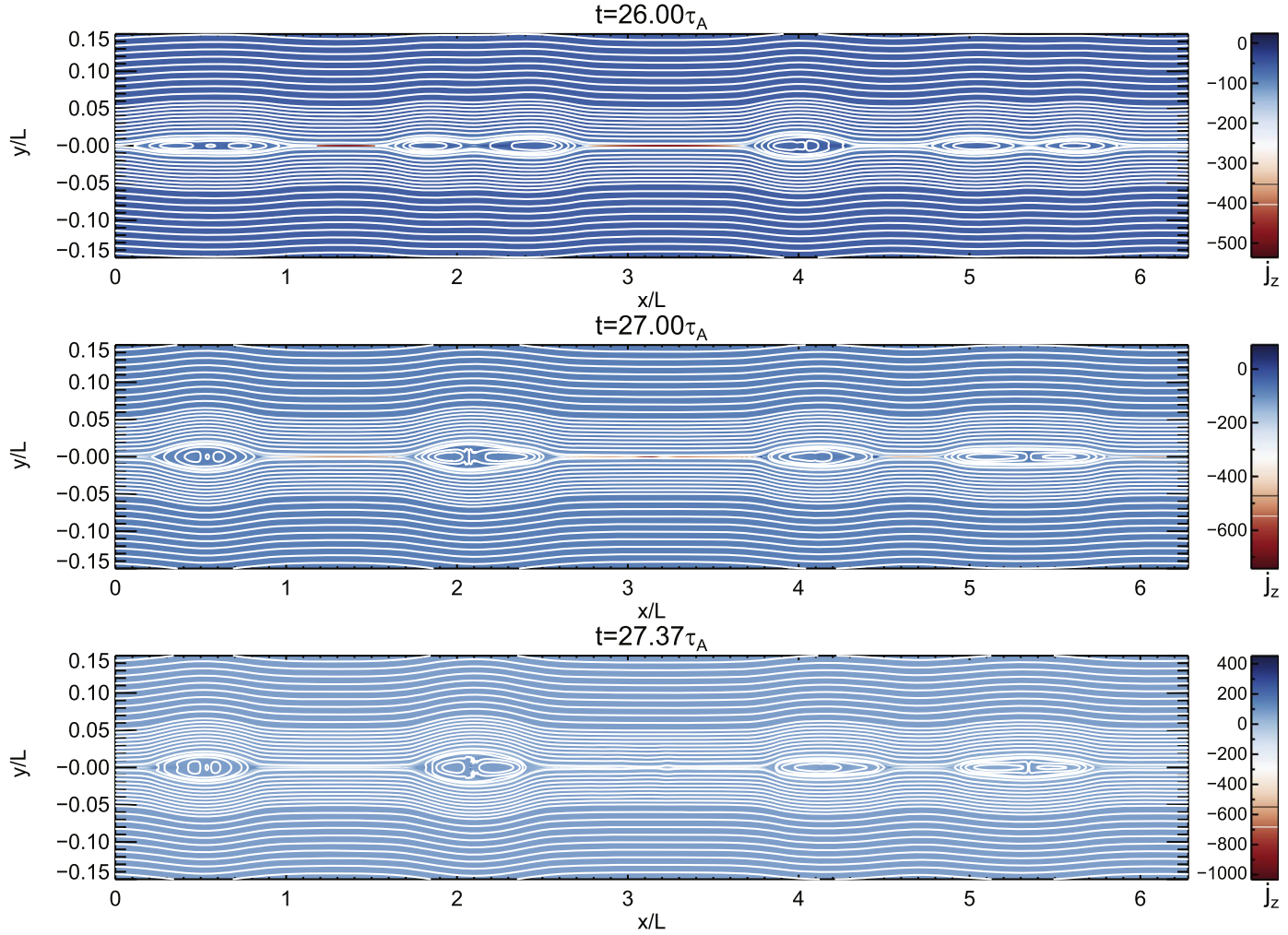

Figure 1. Magnetic field lines and current density are shown at three moments i.e., for $t = 26\tau_A$, $t = 27\tau_A$, and $t = 27\tau_A$ in a collapsing current sheet, from Tenerani et al. (2015b). In the top panel, the central current sheet is lengthening (see e.g., for x/L between 2.7 and 3.7). In the middle panel, the current sheet lengthening has given rise to the plasmoids. In the bottom panel, the x-points between the plasmoids have begun to collapse into a thinner current sheet. The times are normalized to the Alfvén time along the sheet, x, whose total length is 2πL here.

interesting differences from the original (Shibata & Tanuma 2001) ideas. First, the Lundquist number decreases at a much faster rate in each subsequent step, because the geometric progression in the exponential has a ratio 3/4 rather than 5/6. In order for the Lundquist number to fall from say, $S = 10^{12}$ to below 10^4, only 5 steps are required (4 from the initial unstable sheet), i.e., $S_5 = S_1^{(3/4)^4} \simeq 6264$, rather than the previous 9. The total number of plasmoids is also much reduced. In the simulations of Tenerani et al. (2015b, 2016), it was seen that the collapse of x-points does not occur uniformly along the sheet, rather, there is a competition between plasmoid coalescence on the one hand and x-point collapse, in correspondence of the strongest currents, on the other. While for the Shibata model it was obvious that there was originally enough space along the sheet for all of the x-points to collapse and thin to a secondary instability by construction, as the sub-current sheets were of a defined length that summed to the original one; this is not obvious for the Tenerani model. Here we ask that the total number of plasmoids in the half-length, $(N/2)$, times the new instability half-length, L_2, must fit inside the original sheet half-length, L_1. Combining Equation (10) and Equation (20), we obtain

$$N/2 \cdot L_2 \simeq S_1^{1/6}/(2\pi) \cdot L_1 S_1^{-1/4} \leqslant L_1,$$
$$1/(2\pi) S_1^{-1/12} \leqslant 1, \tag{21}$$

which is always satisfied for $S_1 > 1$. The maximum total number of x-points (and therefore plasmoids) that could form in this fractal collapse is given as before by the product of those produced at each step; the total number after M (M-1 secondary)-steps becomes

$$\begin{aligned} N_M &= N_1 \cdot N_2 \cdot ..... \cdot N_M \\ &= \left(\frac{1}{\pi}\right)^M S_1^{1/6} S_2^{1/6} .... S_M^{1/6} \\ &= \left(\frac{1}{\pi}\right)^M S_1^{2/3(1-(3/4)^M)}. \end{aligned} \tag{22}$$

Again, from a realistic viewpoint, M is limited by stabilization at small S, whether due to velocity field or otherwise, somewhere around $S_M \simeq 10^4$, so starting from $S_1 = 10^{12}$, we find that M is at most 5 (actually, 4.8); this leads to a number of islands $N_M \geqslant 0.003 \cdot S_1^{0.5}$. However, if we

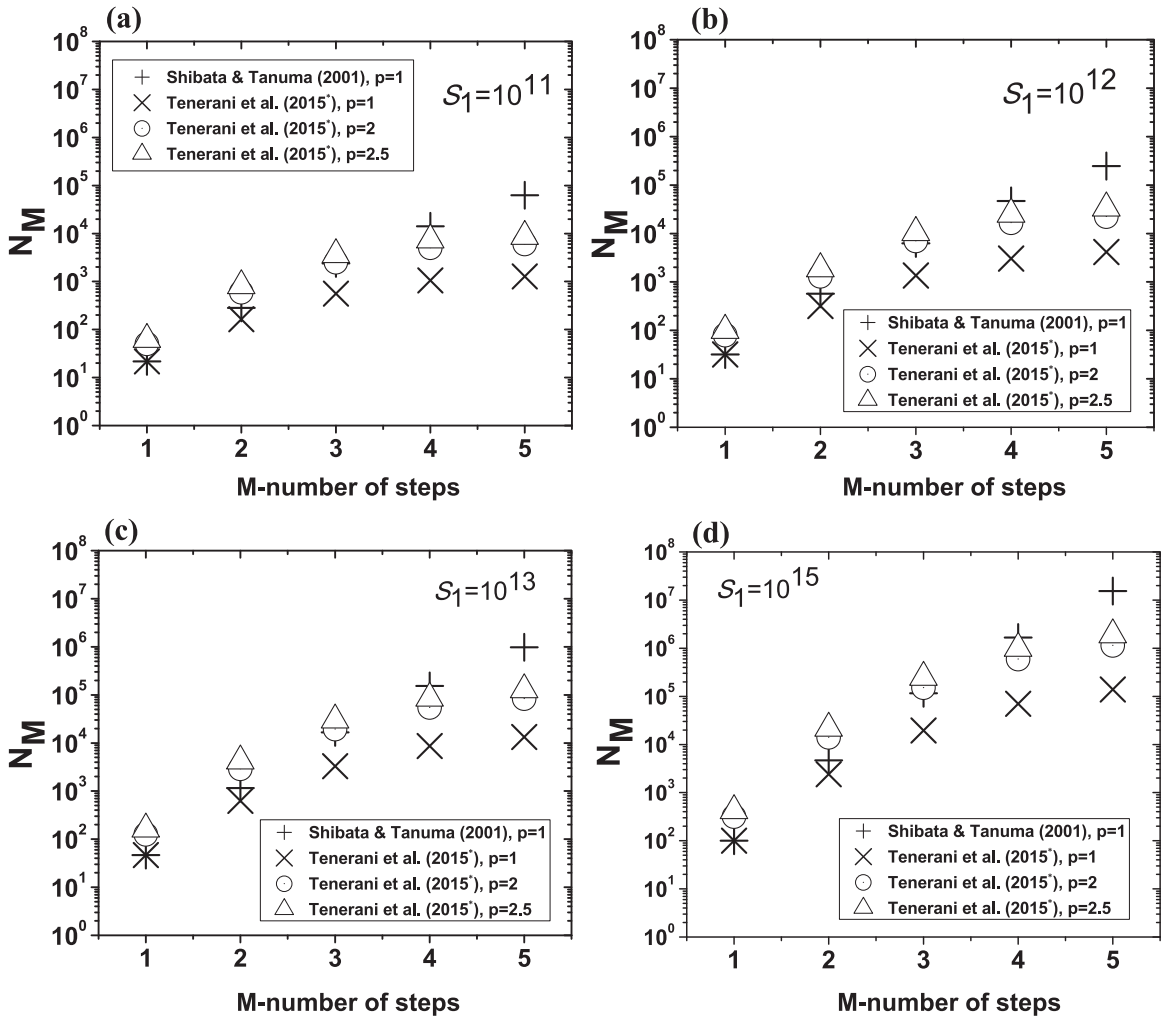

Figure 2. The number of plasmoids (N_M) as a function of M. The calculations for the number of plasmoids are based upon Shibata & Tanuma (2001) and Tenerani et al. (2015b), (a) for $S_1 = 10^{11}$, (b) for $S_1 = 10^{12}$, (c) for $S_1 = 10^{13}$, and (d) for $S_1 = 10^{15}$. In the figure, $\star$-symbol in front of Tenerani et al. (2015a, 2015b) refers to Tenerani et al. (2015b).

assume that only some fraction, i.e., f_i, of the number of plasmoids always make themselves available for the tearing mode instability at the next step, then this number is reduced by a factor $\Pi_{i=2}^{M} f_i$. Although $f_i \leqslant 1$, for the contribution to the number of plasmoids, here f_i is limited by the fact that $f_i n_{i+1} \geqslant 1$, and for a given value of $S = 10^{12}$, $n_1 \simeq 32$, $n_2 \simeq 10$, $n_3 \simeq 4$, $n_4 \simeq 2$, $n_5 \simeq 1$. This means that starting from $S = 10^{12}$, $M = 5$, $f = 0.1$, a reasonable estimate of the total number of plasmoids is $N_M \geqslant 3$. The number of plasmoids as a function of number of steps, and based upon Tenerani et al. (2015b) and $S_1 = 10^{12}$, is shown in Figure 2.

Tenerani et al. (2016) showed that in the hierarchical collapse of current sheets the upstream magnetic field did not tend to be reduced significantly during each step in the self-similar collapse. However, the possibility of a reduced upstream field should not be discounted. This was considered, in the context of secondary tearing excited by a primary macroscopic instability such as the resistive internal kink mode, by Del Sarto & Ottaviani (2017). They found that, assuming a reduction of the upstream field proportional to the thickness of the secondary current sheet, the secondary instability still proceeds faster than the primary resistive mode (arising from the original thick sheet). However, because they did not consider the IT scenario—a central hypothesis required in the asymptotic limit of nearly vanishing resistivity—their secondary instabilities retained a growth rate decaying with increasing Lundquist number, rather than independent of it. For our application here, we are mostly interested in the fact that the reconnecting field is not the upstream field B_0 (defining V_a in the Lundquist number) but only some fraction β of that value, not necessarily proportional to the thicknesses at each step. Changing V_a to βV_a and consequently renormalizing all quantities, the main difference in the number of islands comes via this Lundquist number reduction, each one of which is gaining a factor β, leading to a modification of the scaling relation Equation (20) into

$$S_n = \beta^{6(1-(3/4)^{n-1})} S_1^{(3/4)^{n-1}} \tag{23}$$

and a generalization of Equation (22) yielding the number of x-points or islands after M -steps into

$$N_M = \left(\frac{1}{\pi}\right)^M S_1^{1/6} S_2^{1/6} \ldots S_M^{1/6} = \left(\frac{\beta}{\pi}\right)^M \beta^{-4(1-(3/4)^M)} S_1^{2/3(1-(3/4)^M)}. \tag{24}$$

3.3. Generalized Scaling Laws for Recursive Reconnection (Ideal Tearing)

Although PV14 gave a compelling argument against the requirement of including flows in their study of the tearing in isolated sheet, during the recursive tearing scenario flows are indeed present, and such flows, following the arguments of Shibata & Tanuma (2001), might lead to a slightly different exponent $\alpha \leqslant 1/3$ for the critical inverse current sheet aspect ratios, even considering the $p = 1$ Harris profile. Generalizing the Tenerani et al. (2015b) model to arbitrary α, we find, from Equation (19),

$$a_2/L_2 = \delta_1/L_2 = (L_1/L_2)\cdot S_1^{-(1+3\alpha)/4} = S_2^{-\alpha},\ S_2 = (L_1/L_2)\cdot S_1,$$

implying that

$$S_1^{(\alpha-1)/4} = (L_2/L_1)^{(1-\alpha)} \rightarrow (L_2/L_1) = S_1^{-1/4},$$

just as before. In other words, it remains true that

$$S_{n+1} = S_1^{(3/4)^n}. \tag{25}$$

However, the other scalings, such as the number of islands with Lundquist number, change. Using $a/L \sim S^{-\alpha}$ in Equation (6) leads to $kL \sim S^{(-1+5\alpha)/4}$, and, following the previous procedure, the total number of islands scales as

$$N_M = \left(\frac{1}{\pi}\right)^M S^{(5\alpha-1)(1-(3/4)^M)}. \tag{26}$$

From here, and requesting that we have more than one island, we see that α must obviously satisfy $\alpha > 1/5$ (or the exponent of S would be negative), so it is safe to assume that $1/5 < \alpha < 1/2$. The number of steps is determined only by the values of S so it remains fixed at around 4–5 for any realistic case. Because this calculation only makes sense if the number of islands is $\geqslant 1$ to begin with, the calculation from the Pucci et al. (2018) gives $kL \sim S^{(-1+5\alpha)/4}$, which for $S \simeq 10^{12}$ means that in reality $\alpha \geqslant 0.233$ in order for the process to begin.

The independence of the exponential geometric progression in S on the coefficient α is one interesting aspect. The generalization allowing for magnetic field embedding i.e., the factor β in the Lundquist number at step $i > 1$ leads again to $S_{n+1} = \beta(L_{n+1}/L_n)S_n$ and $S_n = S^{(3/4)^n}\beta^{6(1-(3/4)^n)}$.

The total time (τ_M) for recursion to reach microscopic scales, once the first step has been triggered, i.e., from $n = 2$ to M is

$$\tau_M \simeq \sum_{n=2}^{M} \tau_{A,n},$$

where $\tau_{A,n} = (L_n/L_1)\ \tau_{A1}$. For $\alpha = 1/3$, and neglecting the dependence on β, this leads to

$$\tau_M = S_1^{-1/4}\tau_{A1}[1 + S_1^{-1/4(3/4)} + S_1^{-1/4(3/4+(3/4)^2)} + ...] \sim S_1^{-1/4}\tau_{A1}.$$

For $S = 10^{12}$ that is typical of solar corona, $\tau_5 \sim (5 \times 10^{-4})\tau_A$. Any other value of $\alpha < 1/3$ leads to timescales that are faster.

Let us now come back to the same question, but this time instead of using an arbitrary α and a Harris current sheet, consider different profiles with arbitrary p. The generalization of recursive tearing following Tenerani et al. (2015b, 2016) is simple, following the same steps as above but using Equations (9), (10). The recursive relation for the Lundquist number S now reads

$$S_{n+1} = S_1^{\left(\frac{1+2p}{1+3p}\right)^n}, \tag{27}$$

while the number of x-points generated (assuming that recursive collapse occurs at all x-points) becomes

$$N_M = \left(\frac{1}{\pi}\right)^M S_1^{\frac{1}{2}\left(\frac{1+3p}{1+2p}\right)\left(1-\left(\frac{1+2p}{1+3p}\right)^M\right)}. \tag{28}$$

Note that changing the value of p does not change the recurrence dramatically, as the exponents vary monotonically between $(3/4)^n$ (i.e., for $p = 1$) and $(2/3)^n$ (i.e., for $p \rightarrow \infty$) in the Lundquist number Equation (27) and between $2/3$ ($p = 1$) and $3/4$ ($p \rightarrow \infty$) in the power in front of the parenthesis in the exponent of Equation (28).

Further generalizations follow by relaxing some of the hypotheses considered up to now. Again using $p = 1$, and α for the scaling of the inverse aspect ratio with Lundquist $a/L \sim S^{-\alpha}$, Equation (6) shows that the singular layer thickness will scale with exponent α', such that $\alpha' = \alpha'(\alpha) = -(1 + 3\alpha)/4$. In our stepwise process, we have considered the thickness a_{n+1} to be the inner diffusion layer of the n^{th} tearing step, δ_n in the recursive reconnection based upon the IT scenario of PV14. For a generic α, the equations

$$\frac{a_{n+1}}{L_{n+1}} \sim S_{n+1}^{-\alpha}, \tag{29}$$

and

$$\frac{a_{n+1}}{L_n} \sim S_n^{-\alpha'}, \tag{30}$$

would yield the following scaling laws:

$$\frac{L_n}{L_1} = S_1^{\frac{\alpha-\alpha'}{1-\alpha}[(1-\chi^n)/(1-\chi)]}, \tag{31}$$

$$S_n = S_1^{(1+\varsigma)}. \tag{32}$$

Here, $\chi = (1 - \alpha')/(1 - \alpha)$ and $\varsigma = \frac{(\alpha-\alpha')}{(1-\alpha)}[(1 - \chi^n)/(1 - \chi)]$. So, the scalings derived in Equations (31) and (32) depend on one parameter only.

Consider now a further possibility $L_2/L_1 \sim S_1^{-\beta'}$, expressing the fact that in a secondary collapse the resistivity $\eta_1 \neq \eta$ but rather a function $\eta_1 = \eta_1(\eta)$. We want to investigate what changes in the total number of islands.

The condition which expresses the total number of x-points ($N/2$) that should fit-in, inside the original half-length L for $\alpha = 1/3$, is given in Equation (21). For a generic α this condition becomes

$$\pi N \simeq kL_2 \sim S_1^{-1/4}S_1^{5\alpha/4} \simeq S_1^{1/4(5\alpha-1)} \Rightarrow \frac{S_1^{1/4(5\alpha-1)}}{2\pi}\frac{L_2}{L_1} \leqslant 1. \tag{33}$$

Now, if we generalize $L_2/L_1 \sim S_1^{-\beta'}$ (instead of $L_2/L_1 = S_2/S_1$) we get

$$S_1^{(5\alpha-1-4\beta')} \leqslant (2\pi)^4 \simeq 10^3, \tag{34}$$

so that $\beta' = \beta'(\alpha)$. Now suppose $S = 10^{12}$, then

$$5\alpha - 1 - 4\beta' \leqslant 1/4 \Rightarrow \beta' \geqslant \frac{5}{4}\left(\alpha - \frac{1}{4}\right). \tag{35}$$

Finally, we can compare the value of β' for the case of plasmoid instability in an SP current sheet ($\alpha = 1/2$) and for the IT case ($\alpha = 1/3$)

$$\alpha = 1/2 \Rightarrow \beta' \geqslant 5/16 \tag{36}$$

$$\alpha = 1/3 \Rightarrow \beta' \geqslant 5/48, \tag{37}$$

so that in the SP plasmoid case $L_2/L_1 \leqslant S_1^{-5/16}$ which means, since we considered $S = 10^{12}$, $L_2/L_1 \leqslant 10^{-4}$, while in the IT plasmoid mode case $L_2/L_1 \leqslant S_1^{-5/48}$, so $L_2/L_1 \leqslant 0.03$. A secondary collapse in the IT instability is numerically easier to follow in terms of resolution with respect to the plasmoid case.

4. Summary and Conclusion

Plasmoid-mediated reconnection plays an important role in reconnection dynamics. PV14 proposed the IT model, in which the tearing mode grows with Alfvén timescale at a critical inverse aspect ratio (i.e., $a/L \sim S^{-1/3}$ for the Harris sheet). Tenerani et al. (2015b) developed a magnetic reconnection model describing the nonlinear recursive evolution. Here we have generalized the scalings derived by PV14 and Tenerani et al. (2015b) both to arbitrary current profiles and to different possible stabilizing effects. The recursive plasmoid formation is found to be significantly different assuming a chain of triggering based on an IT scenario with respect to the classical SP fractal reconnection scenario, and this might explain the fact that observations show fewer plasmoids than previously predicted (Takasao et al. 2012). Different types of initial current sheet equilibrium lead to different scalings for the fastest growing mode and potentially different nonlinear evolution (e.g., Tenerani et al. 2015b; Del Zanna et al. 2016; Baty 2017; Pucci et al. 2018). The theoretically subtle differences between recursive models based upon IT and fractal reconnection are discussed.

One of the important results is that the singular layer in an ideally unstable layer is found to be universal and it does not depend upon the details of the initial current profile in the current sheet. The scaling relations including the departure from the Harris-type initial current sheet are derived (see Section 3). We have also derived scaling relation for the number of plasmoids by generalizing recursive reconnection based upon the IT scenario. The number of plasmoids can be compared for $p = 1$, $p = 2$, and $p = 2.5$ (Figure 2); the number of plasmoids for $p = 2$ and $p = 2.5$ show departures from the Harris-type initial current sheet. The present study shows that the departure from the initial, Harris-type current sheet affects the plasmoid formation. The number of plasmoids formed in a recursive, IT (Tenerani et al. 2015b) is much less compared to those predicted by Shibata & Tanuma (2001), see e.g., $M = 5$ of Figure 2. Showing the comparison between number of plasmoids for various cases, we can conclude that the plasmoid dynamics (i.e., x-point collapse combined with the plasmoid formation, merging and intermittent ejection) play a crucial role. Therefore, we can understand that plasmoid dynamics also play an important role in the evolution of the current sheet and fast reconnection. Plasmoids are observed to form in reconnection related events in the solar corona, for example. The number of plasmoids observed is much smaller than that obtained from the scaling relations of the original fractal model. Our work goes some way in explaining this reduction. The latter may also be due to the fact that observational resolution implies that plasmoids are observed only in a deeply nonlinear regime, when significant merging has occurred and their sizes are orders of magnitude greater than those at which reconnection is initiated. Embedding of secondary current sheets, as discussed by Del Sarto & Ottaviani (2017) also leads to a reduction in the number of plasmoids generated. The multiplasmoid instability as observed in nonlinear MHD simulations also depends on the details of the numerical setup (in addition to the obvious Lundquist and Prandtl numbers, always much smaller than realisitic). For example, in the development of secondary instabilities where inflows and outflows are present, a well-defined unique value of the critical Lundquist number beyond which the plasmoid instability is fully developed may not exist, as flows remove the possibility of simple exponential growth rates (Shi et al. 2018). Results also depend on the precise simulation setup including the noise or fluctuations in the initial conditions, as well as boundary conditions (Huang et al. 2017; Shimizu et al. 2017; Shi et al. 2018). Our work has attempted to transcend such limitations by the use of models based on the behavior observed, which are independent of details.

Even though plasmoid instability models have become a very popular subject for the fast reconnection process, a clear understanding of the plasmoid-mediated processes is fundamental as well as vital. The present work provides a guide and predictions to understand the plasmoid instability and recursive reconnection for various scenarios. In addition, the model we describe has implications for reconnection modified turbulence theories (see e.g., Boldyrev & Loureiro 2017). In such theories, the inertial range of turbulence is modified under the assumption that current sheets form naturally as a coherent structure in the cascade, giving rise to a sub-inertial range once the reconnection timescale can compete with the nonlinear eddy turnover time. The fact that when such structures become too thin their growth rates can exceed any appropriate dynamical time clearly justifies considering IT type scenarios within the cascade. An interesting generalization has been recently proposed in Landi et al. (2019). How coherent structures affect inertial range scalings remains a challenging question. In our view a statistical treatment of such current sheets is required, because their current profile is probably not unique. We defer extensions of our analysis to this case to future papers.

A final comment concerns the nonlinear evolution in the presence of kinetic effects, such as the Hall term in the induction equation, that lead directly to an intrinsic 3D behavior. Only few simulations have been carried out in 3D, but it may well be that in the absence of a strong guide field the simple recursive picture presented here will not hold. Although plasmoids may form, their twisting and kinking in three dimensions may lead to a less structured behavior in the subsequent nonlinear evolution (e.g., Landi et al. 2008).

K.A.P.S. gratefully acknowledges the UGC Faculty Recharge Program of Ministry of Human Resource Development (MHRD), Govt. of India and University Grants Commission (UGC), New Delhi as well as the visiting associateship program of Inter University Centre for Astronomy & Astrophysics (IUCAA), Pune. A.H. is supported by his STFC Ernest Rutherford Fellowship grant number ST/L00397X/2 and by STFC grant ST/R000891/1. A.T. and M.V. were supported by the NSF-DOE Partnership in Basic Plasma Science and Engineering award N.1619611 and the NASA Parker Solar Probe Observatory Scientist grant NNX15AF34G.

ORCID iDs

Anna Tenerani https://orcid.org/0000-0003-2880-6084
Andrew Hillier https://orcid.org/0000-0002-0851-5362
Marco Velli https://orcid.org/0000-0002-2381-3106

References

Baalrud, S. D., Bhattacharjee, A., & Germaschewski, K. 2011, PhPl, 18, 092108
Baty, H. 2017, ApJ, 837, 74
Bhattacharjee, A., Huang, Y.-M., Yang, H., & Rogers, B. 2009, PhPl, 16, 112102
Biskamp, D. 1986, PhFl, 29, 1520
Boldyrev, S., & Loureiro, N. F. 2017, ApJ, 844, 125
Cassak, P., & Drake, J. F. 2009, ApJ, 707, 158
Daughton, W., & Roytershteyn, V. 2012, SSRv, 172, 271
Del Sarto, D., & Ottaviani, M. 2017, PhPl, 24, 012102
Del Sarto, D., Ottaviani, M., Pucci, F., Tenerani, A., & Velli, M. 2018, Comptes-rendus de la 21e Rencontre du Non-Linaire Paris (Diderot: Non-Linaire Publications Universit Paris)
Del Sarto, D., Pucci, F., Tenerani, A., & Velli, M. 2016, JGRA, 121, 1857
Del Zanna, L., Landi, S., Papini, E., Pucci, F., & Velli, M. 2016, JPhCS, 719, 012016
Drake, J., & Kleva, R. G. 1991, PhRvL, 66, 1458
Furth, H. P., Killeen, J., & Rosenbluth, M. N. 1963, PhFl, 20, 459
Hesse, M., Birn, J., & Kuznetsova, M. 2001, JGR, 106, 3721
Huang, Y., & Bhattacharjee, A. 2010, PhPl, 17, 062104
Huang, Y.-M., & Bhattacharjee, A. 2010, PhPl, 17, 062104
Huang, Y.-M., & Bhattacharjee, A. 2013, PhPl, 20, 055702
Huang, Y.-M., Bhattacharjee, A., & Sullivan, B. P. 2011, PhPl, 18, 072109
Huang, Y.-M., Comisso, L., & Bhattacharjee, A. 2017, ApJ, 849, 75
Landi, S., Del Zanna, L., Papini, E., Pucci, F., & Velli, M. 2015, ApJ, 806, 131
Landi, S., Franci, L., Papini, E., et al. 2019, arXiv:1904.03903v2
Landi, S., Londrillo, P., Velli, M., & Bettarini, L. 2008, PhPl, 15, 012302
Landi, S., Papini, E., Del Zanna, L., Tenerani, A., & Pucci, F. 2017, PPCF, 59, 014052
Lapenta, G. 2008, PhRvL, 100, 235001
Loureiro, N. F., Schekochihin, A. A., & Uzdensky, D. A. 2007, PhPl, 14, 100703
Loureiro, N. F., Schekochihin, A. A., & Uzdensky, D. A. 2013, PhRvE, 87, 013102
Nishida, K., Nishizuka, N., & Shibata, K. 2013, ApJL, 775, L39
Nishizuka, N., Takasaki, H., Asai, A., & Shibata, K. 2010, ApJ, 711, 1062
Ottaviani, M., & Porcelli, F. 1993, PhRvL, 71, 3802
Parker, E. N. 1957, JGR, 62, 509
Petschek, H. E. 1964, in Proc. AAS-NASA Symp. 425, Physics of Solar Flares, ed. W. N. Hess (Washington, DC: NASA), 425
Pontin, D. I. 2011, AdSpR, 47, 1508
Priest, E. 2014, Magnetohydrodynamics of the Sun (Cambridge: Cambridge Univ. Press)
Pucci, F., & Velli, M. 2014, ApJL, 780, L19
Pucci, F., Velli, M., & Tenerani, A. 2017, ApJ, 845, 25
Pucci, F., Velli, M., Tenerani, A., & Del Sarto, D. 2018, PhPl, 25, 032113
Samtaney, R., Loureiro, N. F., Uzdensky, D. A., Schekochihin, A. A., & Cowley, S. C. 2009, PhRvL, 103, 105004
Servidio, S., Matthaeus, W. H., Shay, M. A., et al. 2010, PhPl, 17, 032315
Shi, C., Velli, M., & Tenerani, A. 2018, ApJ, 859, 253
Shibata, K., & Magara, T. 2011, LRSP, 8, 6
Shibata, K., & Takasao, S. 2016, ASSL, 427, 373
Shibata, K., & Tanuma, S. 2001, EP&S, 53, 473
Shimizu, T., Kondoh, K., & Zenitani, S. 2017, PhPl, 24, 112117
Singh, K. A. P., Hillier, A., Isobe, H., & Shibata, K. 2015, PASJ, 67, 96
Sweet, P. A. 1958, in IAU Symp. 6, Electromagnetic Phenomena in Cosmical Physics, ed. B. Lehnert (Cambridge: Cambridge Univ. Press), 123
Tajima, T., & Shibata, S. 2002, Plasma Astrophysics (Cambridge, MA: Perseus)
Takasao, S., Asai, A., Isobe, H., & Shibata, K. 2012, ApJL, 745, 6
Tanuma, S., & Shibata, K. 2005, ApJL, 628, L77
Tanuma, S., Yokoyama, T., Kudoh, T., et al. 1999, PASJ, 51, 161
Tanuma, S., Yokoyama, T., Kudoh, T., & Shibata, K. 2001, ApJ, 551, 312
Tenerani, A., Rappazzo, A. F., Velli, M., & Pucci, F. 2015a, ApJ, 801, 145
Tenerani, A., Velli, M., Pucci, F., Landi, S., & Rappazzo, A. F. 2016, JPlPh, 82, 5
Tenerani, A., Velli, M., Rappazzo, A. F., & Pucci, F. 2015b, ApJL, 813, L32
Uzdensky, D. A., Loureiro, N. F., & Schekochihin, A. A. 2010, PhRvL, 105, 235002
Yamada, M., Kulsrud, R., & Ji, H. 2010, RvMP, 82, 603
Zweibel, E. G., & Yamada, M. 2009, ARA&A, 47, 291